Nanomedicine: Nanotechnology, Biology, and Medicine
xx (2017) xxx–xxx

nanomedicine
Nanotechnology, Biology, and Medicine

nanomedjournal.com

Near-infrared light-responsive nanoparticles with thermosensitive yolk-shell structure for multimodal imaging and chemo-photothermal therapy of tumor

Song Shen[a,1], Bei Ding[a,1], Shengchang Zhang[a,1], Xueyong Qi[a,*], Kun Wang[d], Jie Tian[d], Yongsheng Yan[d], Yanru Ge[a,*], Lin Wu[b,c,*]

[a]*Department of Pharmaceutics, School of Pharmacy, Jiangsu University, Zhenjiang, China*
[b]*Department of Clinical Pharmacy, Affiliated Hospital of Jiangsu University, Zhenjiang, China*
[c]*Institute of Green Chemistry and Chemical Technology, Jiangsu University, Zhenjiang, China*
[d]*Intelligent Medical Research Center, Institute of Automation, Chinese Academy of Sciences, Beijing, China*

Received 22 October 2016; accepted 22 February 2017

Abstract

Thermosensitive yolk-shell nanoparticles were developed as remote-controlled targeting drug delivery platform for multimodal imaging and combined therapy of cancer. The nanoparticles were fabricated using magnetic Fe_3O_4 nanoparticles as photothermal cores, thermo-responsive poly(N-isopropylacrylamide)-co-1-Vinyl-2-pyrrolidone p(NIPAM-co-NVP) as shells (Fe_3O_4-PNIPAM), with a hollow space between the two layers for loading of chemotherapeutic drug. The magnetic iron oxide nanoparticle cores could absorb and transform light to heat efficiently upon the irradiation of near infrared (NIR) laser, resulting in the shrink of the PNIPAM shell and the release of chemo-drugs. In vivo fluorescence/photoacoustic images demonstrated that Fe_3O_4-PNIPAM nanoparticles could accumulate in the tumor after intravenous injection. Upon the irradiation of the NIR laser, DOX-Fe_3O_4-PNIPAM nanoparticles exhibited outstanding synergistic effect. The tumor inhibition rate increased from 40.3% (DOX-Fe_3O_4-PNIPAM alone) and 65.2% (Fe_3O_4-PNIPAM +NIR) to 91.5%. The results demonstrated that the NIR-responsive nanocarrier offers a novel strategy for cancer theranostics and combined therapy of cancer.

Key words: Photoacoustic imaging; Magnetic iron oxide; Thermoresponsive; Photothermal therapy; Targeting drug delivery

Magnetic iron oxide nanoparticles have attracted extensive interest in biomedical field due to low toxicity, good biocompatibility and high stability in physiological environment. With the unique magnetic properties, magnetic nanoparticles have been widely applied in drug targeting and delivery,[1,2] diagnosis,[3,4] therapy.[5,6] Recently, magnetic iron oxide has been used as photosensitive agent for photothermal therapy (PTT). PTT is a newly emerging technique that employs NIR absorbing materials to mediate the conversion of near-infrared light into heat, and then leads to thermal ablation of cancer cells. Many endeavors have been devoted to the research of NIR absorbing materials such as gold-based nanomaterials,[7–10] carbon-based nanomaterials,[11–14] transition metal dichalcogenides (TMDCs),[15–17] and organic nanoparticles such as melanin,[18–20] Perylene-Diimide.[21] Compared with those NIR absorbing materials, magnetic iron oxide nanoparticles will be prominent photothermal agents due to well biocompatibility, low toxicity, targeting and magnetic resonance imaging. For instance, Chu et al studied the photothermal effect of the Fe_3O_4 nanoparticles with spherical, hexagonal and wire-like shapes for cancer therapy both in vitro and in vivo.[22] Chen et al reported that highly crystallized iron oxide nanoparticles coated

Competing financial interest: The authors declare no competing financial interests.

*Corresponding authors.
E-mail addresses: qixyemail@163.com (X. Qi), geyanru@ujs.edu.cn (Y. Ge), linmeimei1983@163.com (L. Wu).

[1] These authors contributed equally to this work.

http://dx.doi.org/10.1016/j.nano.2017.02.014
1549-9634/

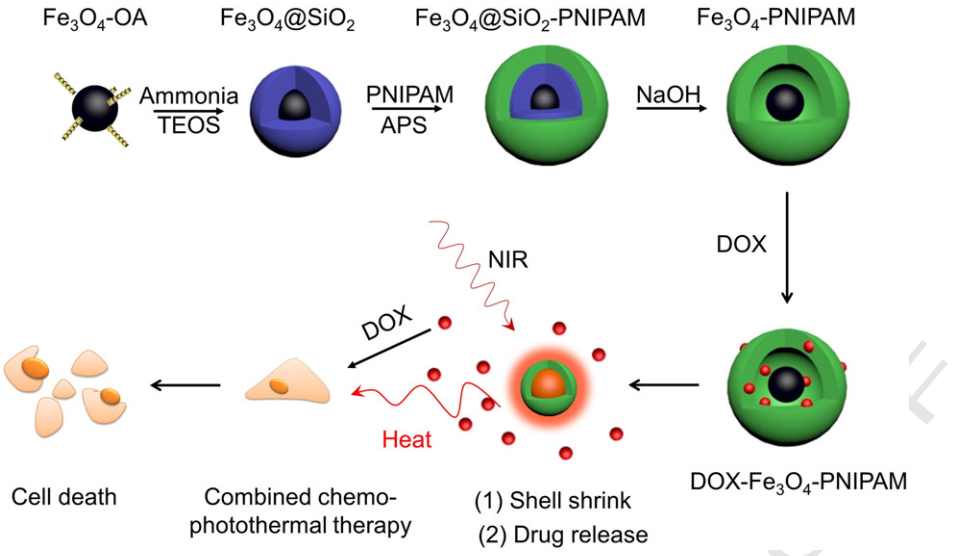

Figure 1. Schematic illustration of the preparation of Fe_3O_4-PNIPAM yolk-shell nanocomposites and NIR-trigger drug release.

with a polysiloxane-containing copolymer could be used as effective mediators for photothermal therapy.[23] We had constructed carboxymethyl chitosan (CMCTS) stabilized Fe_3O_4 nanoparticles with extremely low toxicity for in vivo tumor ablation.[24]

For cancer therapy, traditional chemotherapy suffers from several drawbacks such as poor solubility, non-specificity and adverse side effect. Smart drug delivery systems which are stimuli-responsive, such as thermosensitive microgels, provide the great potential of specific treatment of cancer. With the external heating, the hybrids shrink and lead to the site-specific release of the loaded chemotherapeutic drug in tumor. As one of the most common temperature-sensitive matrix, poly(N-isopropylacrylamide) (PNIPAM) exhibits good biocompatibility and suitable lower critical solution temperature (LCST).[25] Below this critical temperature (T_C), the chains swell and the drug can be loaded. When above the T_C, the chains undergo collapse and the drug is discharged.

Herein, we fabricated yolk-shell structured particles based on Fe_3O_4 particles and stimuli-sensitive poly(N-isopropylacrylamide)-co-1-Vinyl-2-pyrrolidone (p(NIPAM-co-NVP)) matrix. Fe_3O_4-p(NIPAM-co-NVP) (defined as Fe_3O_4-PNIPAM) yolk-shell particles with photothermal and thermo-responsive properties were useful in imaging and chemo-photothermal therapy of tumor. The structure of the particles was schematically illustrated in Figure 1. Thermoresponsive Fe_3O_4@PNIPAM particles have been reported recently.[26,27] However, the reported thermoresponsive particles were prepared by coating PNIPAM directly onto the surface of the Fe_3O_4 instead of yolk-shell structure which could increase the loading capacity of drug by the interstitial space between the outer shell and the inner core. The prepared nanocomposites exhibited favorable magnetic property and outstanding NIR optical absorbance, and thus offered the contrasts in magnetic resonance imaging (MRI) and multispectral optoacoustic tomography (MSOT) imaging. Upon the irradiation of NIR laser, drug release obviously enhanced. Synergistic anticancer effect was observed both in vitro and vivo experiment, indicating the potential of the nanocomposites for specific therapy of cancer.

Methods (refer to the supplementary information for details)

Yolk-shell structured Fe_3O_4-PNIPAM nanoparticles were synthesized and characterized. In vivo experiments were performed in compliance with the Jiangsu University Animal Study Committee's requirements for the care and use of laboratory animals in research.

Results

Synthesis, characterization and thermosensitive property of nanocomposite

As illustrated in the transmission electronic microscopy (TEM), the Fe_3O_4 nanoparticles had a uniform size with an average diameter of ~25 nm (Figure 2, *A*, S1). When silica layer was introduced onto the Fe_3O_4 to form Fe_3O_4@SiO_2 nanoparticles, these nanoparticles remained uniform shapes with the mean diameter of ~65 nm (Figure 2, *B*, S1). The Fe_3O_4@SiO_2 particles coated with thermosensitive layer had been confirmed by TEM image (Figure 2, *C*). Thermosensitive layer thickness was about 50 nm (Figure 2, *C*, S1). Figure 2, *D* revealed a noticeable yolk-shell structure after SiO_2 layer was etched. The formation the nanoparticles can also be verified by thermo-gravimetric analysis (TGA). As shown in Figure S2a, the weight loss of ~45% mainly attributed to the decomposition of oleic acid on the surface of Fe_3O_4. With the coating of SiO_2, the weight loss decreased to about 25%. Then over 40% of weight loss was found after the introduction of p(NIPAM-co-NVP). The etching of SiO_2 further increased the weight loss to about 55%. The TGA results indicate the successful construction of the yolk-shell structure.

Fe_3O_4-p(NIPAM-co-NVP) (defined as Fe_3O_4-PNIPAM) yolk-shell particles showed the absorption at NIR region (700 ~ 850 nm). Drug-loaded particles (DOX-Fe_3O_4-PNIPAM) displayed a UV–vis absorption peak at 490 nm, which was the characteristic of free DOX (Figure 3, *A*). The thermosensitive

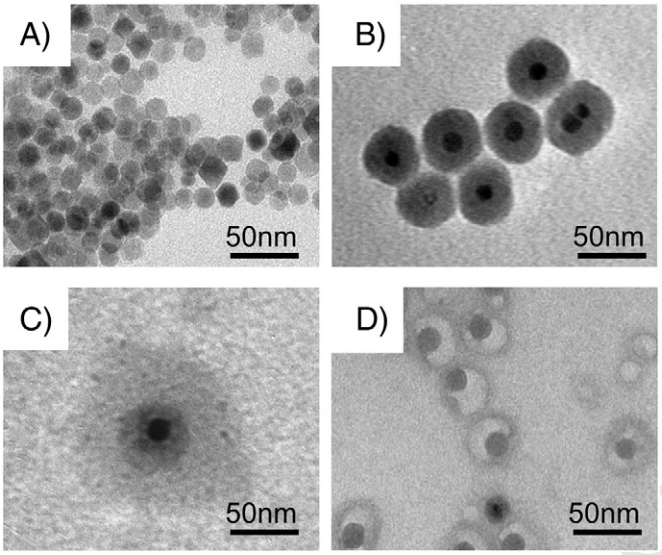

Figure 2. TEM images of **(A)** Fe_3O_4-OA nanoparticles; **(B)** Fe_3O_4@SiO_2 core-shell nanoparticles; **(C)** Fe_3O_4@SiO_2-PNIPAM trilayer composites; **(D)** Fe_3O_4-PNIPAM yolk-shell nanoparticles after SiO_2 layer was etched.

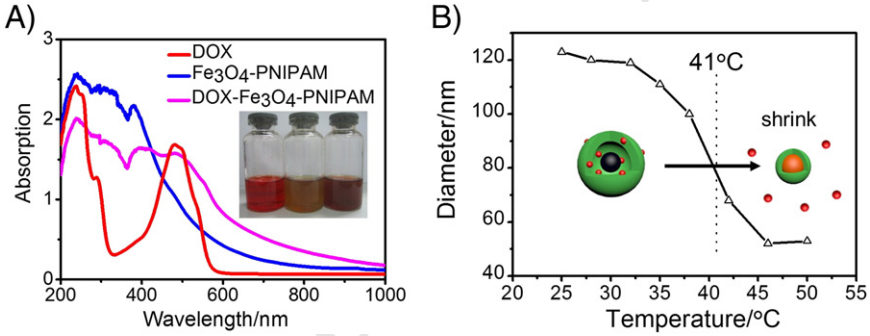

Figure 3. **(A)** Absorbance spectra of free DOX (red, 90 μg mL^{-1}), Fe_3O_4-PNIPAM yolk-shell particles (blue, 50 μg mL^{-1}), and DOX-Fe_3O_4-PNIPAM particles (pink, 60 μg mL^{-1}); **(B)** Variation of the diameters of the Fe_3O_4-PNIPAM yolk-shell particles as a function of temperature.

property of Fe_3O_4-PNIPAM yolk-shell particles had been determined by particle size analyzer (Figure 3, *B*). The LCST was measured in the process of raising temperature from 25 to 50 °C. Rapid decline of the average diameter was observed around 41 °C, indicating the LCST of the thermosensitive particles.

MRI and T_2 relaxivity measurement

The T_2-weighted MR images of Fe_3O_4-PNIPAM nanoparticles were investigated by a 3.0 T clinical MR scanner. Obvious darkening effects were observed with the increase of iron concentration (Figure 4, *A*). Linear fitting of the T_2 relaxation rate ($1/T_2$) as a function of Fe concentration was carried out (Figure 4, *B*), exhibiting a transverse relaxivity (r_2) of 14.96 $mM^{-1}S^{-1}$. The darkening effects were also observed in MR images of cells. The signal intensity showed significant decrease with the increasing of iron concentration (Figure 4, *C*). These results indicate the potential of Fe_3O_4-PNIPAM nanoparticles as contrast agents for MR imaging.

Photothermal effect of the Fe_3O_4-PNIPAM particles

Figure 4, *D* revealed the photothermal temperature images of Fe_3O_4-PNIPAM nanocomposites suspensions with different concentration irradiated by NIR laser. The temperature rising rate and final temperature depended on the concentration and irradiation time. It was shown that the temperature could be increased from 27 to 80 °C at a 200 μg mL^{-1} concentration within 8 min. The temperature rising rate became slower when the concentration decreased. As control, a negligible temperature increase was observed for the water with NIR irradiation at the same NIR intensity (Figure 4, *E*).

Photoacoustic imaging in vitro

The application of magnetic iron oxide nanoparticles as a probe for photoacoustic imaging was investigated in vitro. As shown in Figure 4, *F*, Fe_3O_4-PNIPAM nanoparticles irradiated by NIR laser showed strong PA signals than that without NIR laser. The same result was found in the cell experiment. After

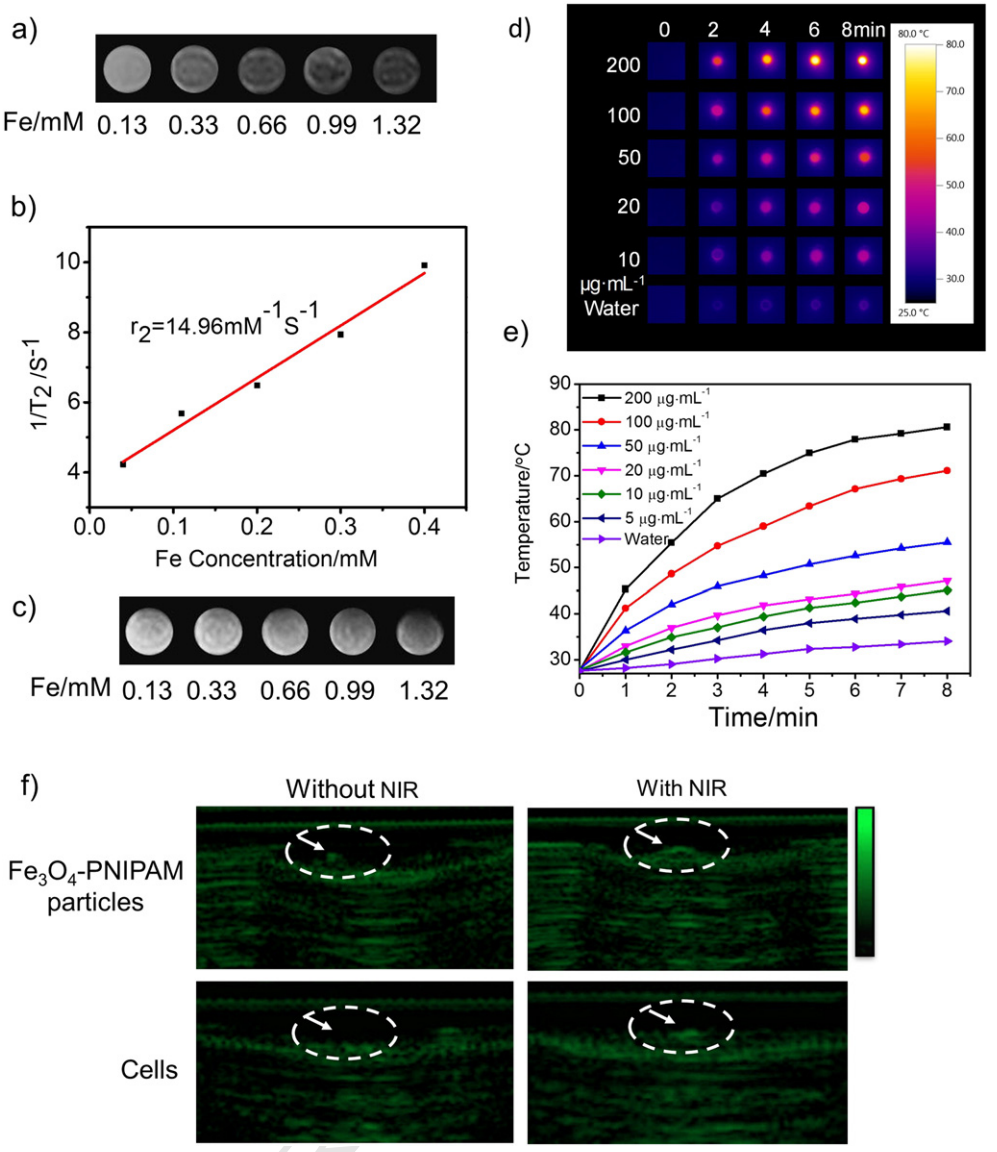

Figure 4. **(A)** MR images of Fe_3O_4-PNIPAM nanoparticles at different Fe concentration; **(B)** T_2 relaxation rate ($1/T_2$) of Fe_3O_4-PNIPAM nanoparticles as a function of iron concentration (mM); **(C)** MR images of MCF-7 cells incubated with the Fe_3O_4-PNIPAM nanoparticles at different Fe concentration; **(D)** Photothermal images of Fe_3O_4-PNIPAM nanoparticles at various concentration with different exposure time; **(E)** Photothermal temperature curves of Fe_3O_4-PNIPAM nanoparticles at various concentration with different exposure time; **(F)** Photoacoustic images before and after NIR irradiation: Fe_3O_4-PNIPAM particles and the cells treated with Fe_3O_4-PNIPAM nanoparticles.

incubation with Fe_3O_4-PNIPAM nanoparticles for 24 h, photoacoustic signal could be detected in the cells upon NIR irradiation, while no obvious signal was detected in the cells without NIR laser irradiation. These results demonstrate the potential of Fe_3O_4-PNIPAM nanoparticles using as good photoacoustic imaging probe.

DOX loading and laser-trigger drug release

Loading behaviors of DOX in Fe_3O_4-PNIPAM yolk-shell nanoparticles (abbreviated as DOX-Fe_3O_4-PNIPAM) were investigated. As shown in Figure 5, *A*, the loading capacity of DOX in Fe_3O_4-PNIPAM nanoparticles reached 25%, while the loading capacity in Fe_3O_4@SiO_2-PNIPAM core-shell nanoparticles was below 10% (Figure 5, *A*). The loading capacity of DOX in Fe_3O_4-PNIPAM nanoparticles was also verified by the TGA (Figure S2b). The increased loading capacity should be attributed to two reasons. One is the etching of SiO_2 layer, which reduces the weight of the particles. The other is the hollow interlayers formed between Fe_3O_4 and PNIPAM. After the deposition of DOX, the color of the DOX-Fe_3O_4-PNIPAM changed from yellowish to henna (Figure 3, *A*). DOX-Fe_3O_4-PNIPAM displayed a characteristic DOX absorption peak at ~490 nm (Figure 3, *A*).

NIR-triggered DOX release from DOX-Fe_3O_4-PNIPAM yolk-shell nanoparticles was performed in water and phosphate buffer saline (PBS) solution at different pH values (Figure 5, *B*). After first treated with NIR laser irradiation for 5 min, the cumulative release of DOX increased from 3.6% to 10% at

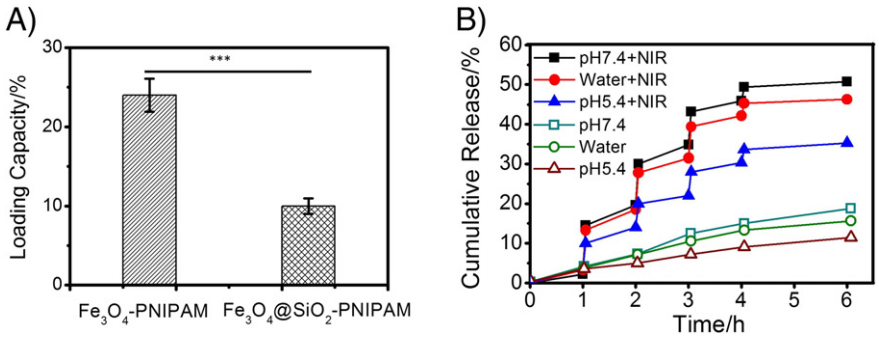

Figure 5. **(A)** Drug loading capacity of Fe_3O_4-PNIPAM yolk-shell nanoparticles and Fe_3O_4@SiO_2-PNIPAM core-shell nanoparticles (*** $P < 0.001$); **(B)** DOX release from DOX-Fe_3O_4-PNIPAM yolk-shell nanoparticles with or without NIR laser irradiation at water and PBS solution with different pH.

pH 7.4 and from 2.2% to 14.5% at pH 5.4. However, the release rate slowed down when the laser was switched off during the following 1 h of incubation. Similar results were found when the release protocol was repeated in the following experiments. With the NIR irradiation for 6 h, the percentages of cumulative release reached 35.3% and 50.7% at pH 7.4 and pH 5.4, respectively. In contrast, only less than 20% of DOX was released from the nanoparticles without NIR laser. Similar NIR sensitive release profile of DOX was observed in water. These results indicate that pulsatile release of DOX from Fe_3O_4-PNIPAM nanoparticles could be triggered by external NIR laser. Upon the irradiation of the NIR light, overheat was generated on the surface of the iron oxide nanoparticles during the photo-thermal conversion, which leaded to the shrink of the thermosensitive yolk-shell and the squeeze of drug from the hollow interlayers. The pH dependency drug release was also observed that more DOX was released under pH 5.4 than in pH 7.4 media during the same period. This trend was attributed to the increased hydrophilicity and higher solubility of DOX at lower pH, which reduced the electrostatic interaction between DOX and Fe_3O_4-PNIPAM nanoparticles.

Cellular uptake in vitro

To investigate the effects of Fe_3O_4-PNIPAM particles on intracellular localization of DOX, the intracellular behaviors in MCF-7 cells (human breast carcinoma cell line) were studied by confocal microscopy (Figure 6). Red fluorescence from DOX and blue fluorescence from Hoechst 33,342 for cell nucleus staining had been observed. After incubation with free DOX for 15 min, red fluorescence could be detected in the nuclei, suggesting fast diffusion and interlization of free DOX. For DOX-Fe_3O_4-PNIPAM, increased fluorescence intensity was observed as the incubation time extended, indicating the time-dependent cellular uptake. After 15 min and 1 h incubation, DOX-Fe_3O_4-PNIPAM particles were mainly located in the cytoplasm but out of the nuclei. This results suggest that Fe_3O_4-PNIPAM particles could deliver DOX to tumor cells efficiently and they could not transfer the drug into the nuclei. However, DOX fluorescence was observed in the nuclei after 4 h incubation. This phenomenon mainly due to the time- and pH-dependent drug release within cells and the detached DOX diffused into the nuclei.

To further study the pulsatile DOX release from nanoparticles induced by NIR, MCF-7 cells were incubated with pretreated DOX-Fe_3O_4-PNIPAM for 15 min. As shown in the Figure S3, brighter fluorescence was observed after NIR irradiation compared with that without pretreatment. After 1 h incubation, strong fluorescence in nuclei could be detected while no obvious fluorescence was found in the cells without NIR treatment, indicating the fast release of DOX upon NIR irradiation. 4 h later, both the fluorescence in nuclei and cytoplasm became stronger, showing a time dependent uptake.

Targeted therapy in vitro

To confirm the targeting ability of Fe_3O_4-PNIPAM nanoparticles, MCF-7 cells were incubated with DOX-Fe_3O_4-PNIPAM nanoparticles in the presence of a magnet. After NIR laser irradiation and incubation for another 24 h, the dead cells were stained blue by treating them with 0.4% trypan blue for 10 min (Figure S4). Cell death is shown as a blue circular spot that matches the magnet spot size. No destruction of the cells outside the magnet spot was observed, even after exposure to a power of 3 W cm^{-2} for 8 min. These results clearly demonstrate that Fe_3O_4-PNIPAM nanoparticles which absorb NIR radiation could be used as promising targeting vectors.

Cytotoxicity in vitro

The cytotoxicity of Fe_3O_4-PNIPAM particles with and without NIR irradiation was investigated on MCF-7 cells by standard MTT assays. As shown in Figure S5, no significant cytotoxicity was observed after the cells were exposed to nanoparticles without NIR laser; cell viability was around 90%; even the concentration of Fe_3O_4-PNIPAM was as high as 500 μg mL^{-1}. In contrast, a remarkable decrease in cell viability was found after exposure to NIR laser, over 70% of the cells were killed when the cells were treated with Fe_3O_4-PNIPAM at the concentration of 500 μg mL^{-1}. No significant influence of NIR laser on cell viability was observed even the irradiation time reached 10 min (Figure S6).

DOX-Fe_3O_4-PNIPAM exhibited dose-dependent cytotoxicity against MCF-7 cells and BRL-3A cells (Figure S7). About 72% of MCF-7 cells and 77% of BRL-3A cells (rat liver cell line) were killed by DOX-Fe_3O_4-PNIPAM at an equivalent DOX concentration of 10 μg mL^{-1}. However, free DOX exhibited

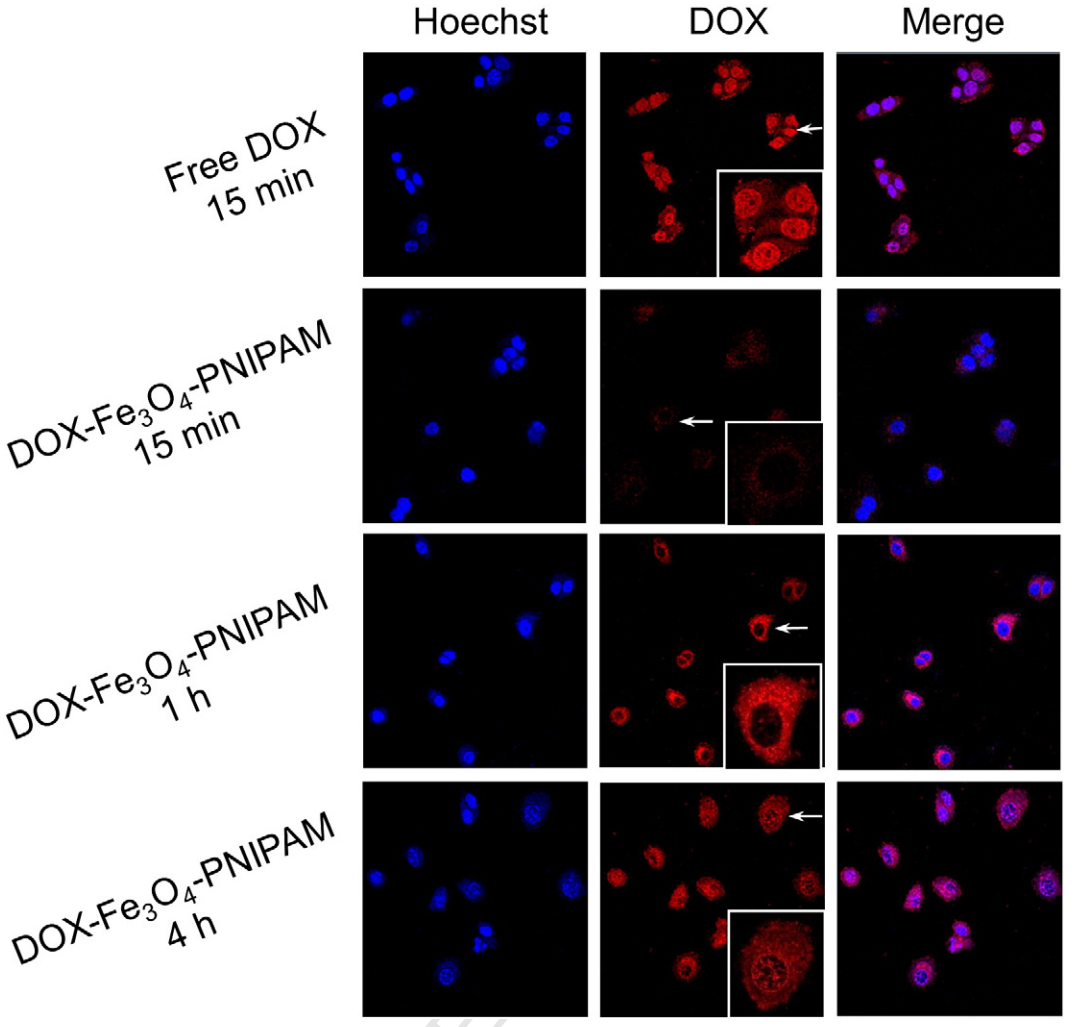

Figure 6. Cell uptake of free DOX or DOX-Fe_3O_4-PNIPAM for 15 min, 1 h, 4 h. Blue fluorescence of Hoechst 33,342 indicated the nuclei and red fluorescence indicated the DOX.

higher toxicity, with over 85% cell killed at the same drug concentration. The lower cytotoxicity of DOX-Fe_3O_4-PNIPAM could be attributed to retained drug release inside cells and the poor efficiency of nuclei targeting drug delivery. Upon NIR irradiation, no obvious influence on the cytotoxicity of free DOX was observed. However, after NIR irradiation (the temperature during the experiment was remained below 42 °C), DOX-Fe_3O_4-PNIPAM showed notably enhanced cell killing effects than that without NIR laser irradiation. The significantly enhanced cell-killing effects revealed the triggered drug release from the nanoparticles and significant photothermal ablation of Fe_3O_4-PNIPAM. Thus, combined treatment exhibited better therapeutic effect than photothermal therapy or chemotherapy alone.

Biodistribution measurement

To demonstrate the in vivo biodistribution behavior of Fe_3O_4-PNIPAM nanocomposites, we injected Fe_3O_4-PNIPAM-ICG intravenously into tumor bearing mice using free ICG as control. The mice were imaged by the Maestro in vivo imaging system at certain time points. Figure 7, *A* shows the fluorescent images of the mice after the injection of free ICG and Fe_3O_4-PNIPAM-ICG for 4 h, 8 h, 12 h, 24 h and 48 h. Tumor injected with Fe_3O_4-PNIPAM-ICG showed increased signals over time, with brightest fluorescence at 24 h post injection, indicating the high accumulation of Fe_3O_4-PNIPAM particles in the tumor. Besides, Fe_3O_4-PNIPAM-ICG also exhibited prolonged retention effect in tumor, which might be attributed to the enhanced permeability and retention effect (EPR). In contrast, free ICG was quickly eliminated from the body although it could distribute in tumor efficiently at the initial site of injection. To further investigate the biodistribution of the particles, major organs of the mice were harvested and imaged. As shown in Figure 7, *B*, ICG from Fe_3O_4-PNIPAM-ICG particles were mainly accumulated in the tumor at 24 h post-injection. As a control, free ICG which exhibited a high accumulation at liver and kidney showed a poor ability to accumulate at tumor owing to the absence of the targeting effect. These results are in accordance with the in vivo biodistribution in Figure 7, *A*. T_2-weighted MR imaging was also conducted after intravenous injection of Fe_3O_4-PNIPAM, showing obvious darkening effects in tumor after injection (Figure 7, *C*). MRI results not only indicate the

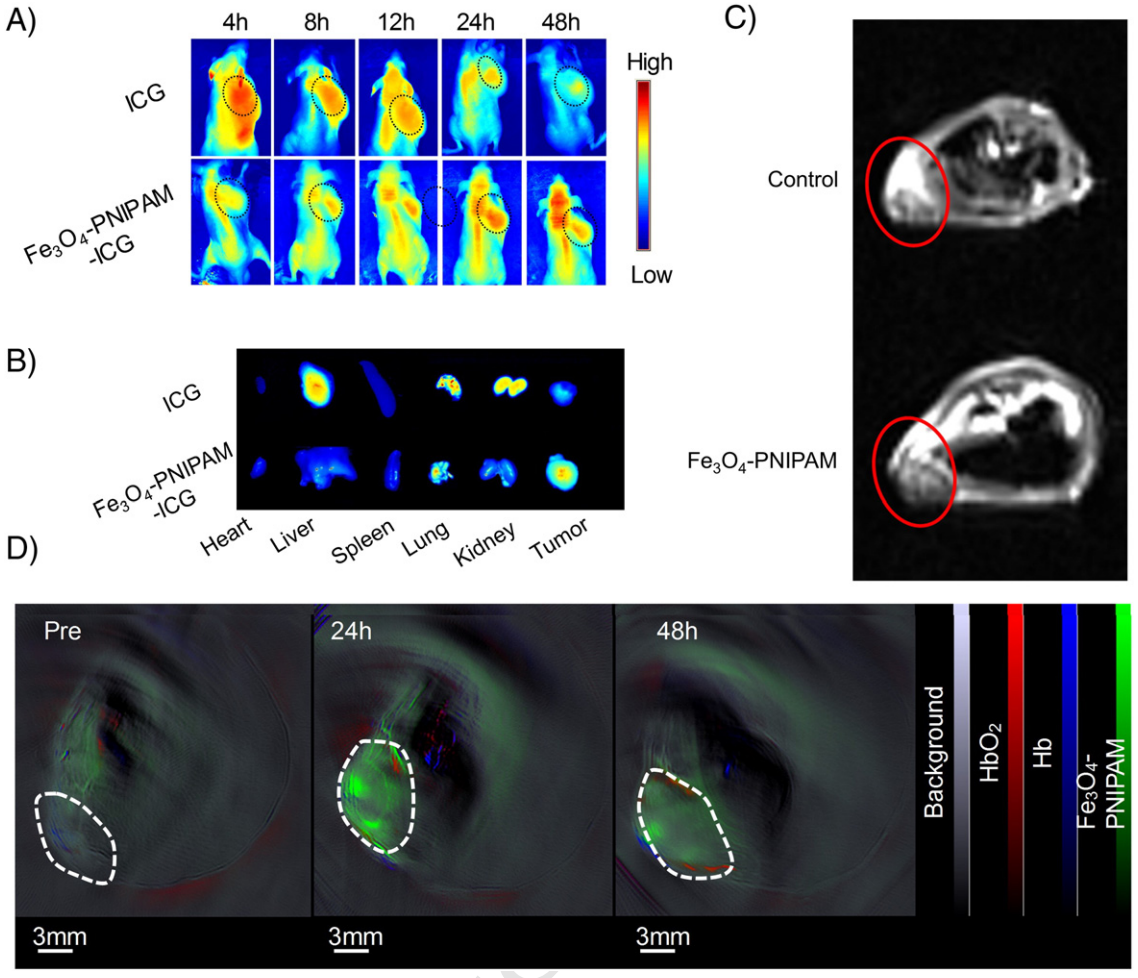

Figure 7. In vivo imaging and biodistribution of Fe_3O_4-PNIPAM particles. Fluorescence images showing the in vivo imaging **(A)** and ex vivo **(B)** biodistribution of free ICG (200 μL, 200 μg·mL^{-1}) and Fe_3O_4-PNIPAM-ICG (200 μL, 10 mg mL^{-1}) after intravenous injection for 24 h. **(C)** In vivo T_2-weighted MR images of S180 tumor-bearing mice obtained 24 h after intravenous injection of saline and Fe_3O_4-PNIPAM-ICG (200 μL, 10 mg mL^{-1}); **(D)** MSOT images of S180 tumor-bearing mouse before and after injection of Fe_3O_4-PNIPAM (200 μL, 10 mg mL^{-1}) showing overlaid HbO_2, Hb and Fe_3O_4-PNIPAM signals.

potential of Fe_3O_4-PNIPAM as MRI contrast agent but also the good tumor targeting ability. The high accumulation of Fe_3O_4-PNIPAM-ICG in the tumor might be attributed to the prolonged blood circulation time and the enhanced permeability and retention effect (EPR) of the tumor.

The biodistribution of Fe_3O_4-PNIPAM particles was also investigated by MSOT Imaging. The spatial distributions of Fe_3O_4-PNIPAM particles, hemoglobin (Hb) and oxyhemoglobin (HbO_2) in S180 tumor-bearing mice were reconstructed by MSOT (Figure 7, *D*). It was shown that the Hb and HbO_2 signals that reflect the locations of blood vessels mainly located in the outer layer of the tumor. Strong photoacoustic signals of were observed in the tumor after injection of Fe_3O_4-PNIPAM particles for 24 h, indicating the diffusion of Fe_3O_4-PNIPAM particles from vessels to tumor matrix. The intensity of the signal decreased obviously after injection for 48 h, suggesting the elimination of Fe_3O_4-PNIPAM from tumor. In contrast, no obvious PA signal was observed in the S180 tumor before tail-vein injection of Fe_3O_4-PNIPAM particles. These data indicate not only the remarkable tumor targeting effect of the nanoparticles but also the great potential of Fe_3O_4-PNIPAM as nanoprobe for PAI.

Combined photothermal-chemotherapy in vivo

Considering the obvious NIR triggered drug release in vitro and the remarkable tumor targeting effect, the in vivo synergistic efficacy of DOX-Fe_3O_4-PNIPAM was studied. DOX, Fe_3O_4-PNIPAM and DOX-Fe_3O_4-PNIPAM solutions were injected through the tail vein into S180 tumors bearing ICR mice, and then the tumors were treated with NIR at 24 h post-injection. With NIR irradiation, the tumor temperature of Fe_3O_4-PNIPAM injected group increased rapidly to reach 50 °C within 5 min (Figure 8, *A*), while the tumor temperature of saline group remained below 42 °C during the entire treatment. During the therapeutic period, the changes in the tumor volume were monitored. As shown in Figure 8, *B*, the growth of tumor treated with free DOX and DOX- Fe_3O_4-PNIPAM was inhibited. However, the tumor inhibition rates were only 35.6% and 40.3% respectively. Besides, no significant difference in tumor growth

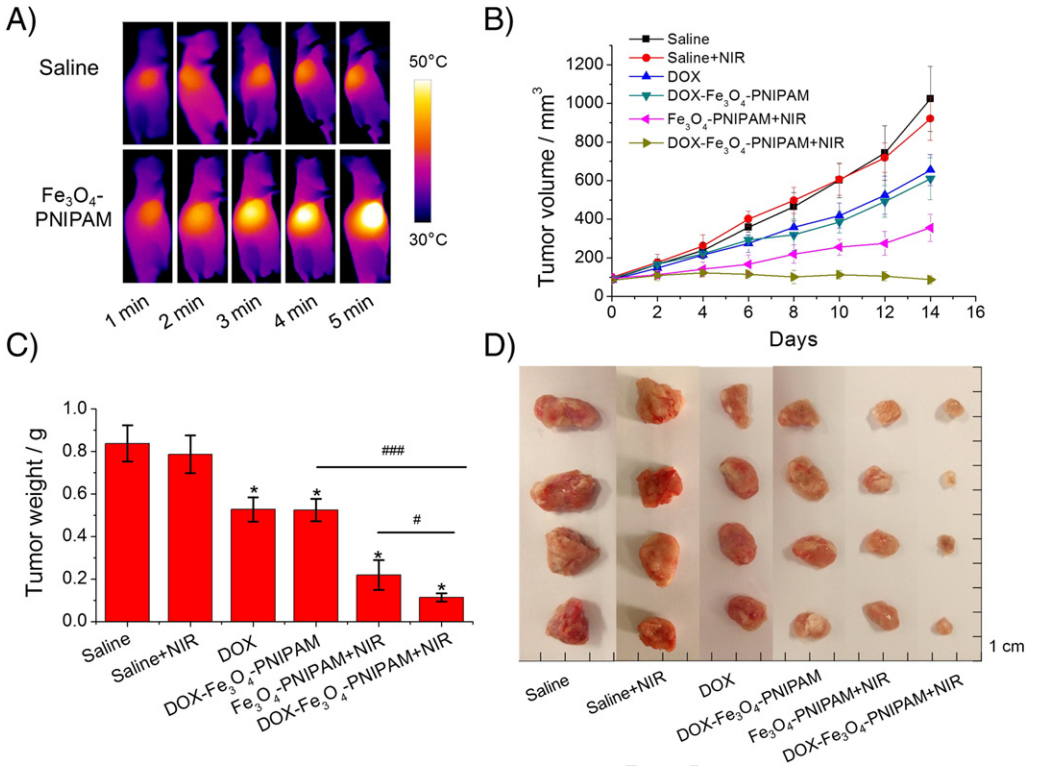

Figure 8. Combined chemo-phototherapy in vivo. **(A)** Thermographic images of saline-injected (200 μL) (Control) and Fe_3O_4-PNIPAM-injected (200 μL, 10 mg mL^{-1}) (treatment) tumor-bearing mice under 808 nm laser irradiation at a power density of 1.5 W cm^{-2} with different time. **(B)** Tumor growth curves of S180 tumor following the different treatments. **(C)** Average weights of tumors at the end of 14 d treatments (*$P < 0.05$, #$P < 0.05$, ###$P < 0.001$, by ANOVA with Tukey's post-test). **(D)** Photos of the tumors collected from different groups of mice at the end of treatments (day 14).

inhibition between DOX and DOX- Fe_3O_4-PNIPAM group was observed, although the DOX-loaded Fe_3O_4-PNIPAM particles exhibited superior tumor targeting effect. This result may be explained by sustained release of DOX from Fe_3O_4-PNIPAM particles inside the tumor cells. However, significant tumor suppression effect was observed while the DOX-Fe_3O_4-PNIPAM treated mice were irradiated with NIR, indicating the emergence of the synergistic therapeutic effect of hyperthermia and chemotherapy. The tumor inhibition rate increased remarkably from 40.3% to 91.5%. In contrast, Fe_3O_4-PNIPAM particles without DOX exposed to NIR group exhibited lower tumor inhibition rate of 65.2%, which was in accordance with their cytotoxic results in vitro as shown in Figure S7. This result indicates the burst drug release controlled by NIR. When the treatments finished, the mice were sacrificed and the tumors were collected and weighed. As shown in Figure 8, *C, D*, combined therapy group displayed significant difference in tumor mass compared with chemotherapy or photothermal therapy alone (DOX-Fe_3O_4-PNIPAM, Fe_3O_4-PNIPAM + NIR), $P < 0.05$. The above in vivo results demonstrated that DOX-Fe_3O_4-PNIPAM + NIR could generate much greater antitumor efficiency than free DOX or PTT alone, which implied the good clinical application potential of this remote-controlled drug delivery system.

Discussion

Yolk-shell nanostructures have been extensively studied and applied in biological areas such as drug delivery and multifunctional theranostic platforms,[28] owing to their unique properties, such as low density, excellent loading capacity, and easy functionalization. Various yolk-shell particles have been fabricated, such as Au@SiO_2,[29] Ag@Carbon@Silica,[30] and SiO_2@SiO_2.[31] Although some progress in the synthesis has been achieved, to fabricate stimulate-responsive nanoparticles is still a challenge. Here, we constructed NIR sensitive nanoparticles with yolk-shell structure, which could increase the drug loading capacity significantly from ~9% to 25% also realize burst release upon the irradiation of NIR.

The accumulation of nanoparticles in tumor is essential for specific therapy of cancer. For different particles, the time needed to reach the tumor site is different. Liu reported that the multifunctional nanoparticles with particle size of ~220 nm could accumulated in tumor 2 h post injection.[32] However, the magnetic particles we prepared needed 12–16 h to accumulate in the tumor. The coating such as carboxymethyl chitosan (CMCTS),[24] hyaluronic acid (HA),[33] has little influence on the biodistribution, while the particle size displayed a significant influence.[34]

As an MRI contrast agent, iron oxide has been used for over a decade in the clinic. In this study, we found that it can also be applied for PA imaging. Compared with MRI, PA imaging has much lower cost and higher sensitivity to tissue. The outline of the tumor and the blood vessels around it could be seen from the imaging, which indicated Fe_3O_4-PNIPAM particles as PA imaging agent could be used for tumor diagnosis.

Herein, we fabricated novel yolk-shell thermosensitive nanoparticles using the silica-etching method. As drug carrier, the nanoparticles demonstrated high drug loading capacity

owing to the unique yolk-shell structure of Fe_3O_4-PNIPAM particles. The hollow interior of the nanoparticles allowed significant increase in effective space for DOX deposition, resulting in 2.5-fold increase in DOX payload compared with solid Fe_3O_4@SiO_2-PNIPAM particles. The phase transition temperature of the thermosensitive polymer was 41 °C, which could be used to realize pulsatile drug release of DOX from Fe_3O_4-PNIPAM particles using NIR light as the external stimulus. Beyond that, we further employed Fe_3O_4-PNIPAM particles as theranostics probe for in vivo PAI to real-time monitor the biodistribution of the carrier. With a long blood circulation half-life, the Fe_3O_4-PNIPAM nanoparticles demonstrated surprisingly tumor accumulation by the EPR effect and magnetic targeting effect after intravenous injection. In the combined treatment experiments, Fe_3O_4-PNIPAM nanoparticles displayed enhanced synergistic effect both in vivo and vitro, without expressing obvious cytotoxicity. The novel yolk-shell thermosensitive Fe_3O_4-PNIPAM particles offer an innovative targeting drug delivery platform for multimodal imaging and combined therapy of cancer.

Acknowledgments

This study was supported by the National Natural Science Foundation of China (81172999, 81503017), Natural Science Foundation of Jiangsu Province (BK20150534), Senior Talent Foundation of Jiangsu University (No. 14JDG181), A Project Funded by the Priority Academic Program Development of Jiangsu Higher Education Institutions (PAPD), China Postdoctoral Science Foundation (2015 M580404) and Jiangsu Planned Projects for Postdoctoral Research Funds (No. 1402075B).

Appendix A. Supplementary data

Supplementary data to this article can be found online at http://dx.doi.org/10.1016/j.nano.2017.02.014.

References

1. Yang Y, Guo X, Wei K, Wang L, Yang D, Lai L, et al. Synthesis and drug-loading properties of folic acid-modified superparamagnetic Fe_3O_4 hollow microsphere core/mesoporous SiO_2 shell composite particles. *J Nanopart Res* 2014;**16**:1-10.
2. Sadighian S, Rostamizadeh K, Hosseini-Monfared H, Hamidi M. Doxorubicin-conjugated core–shell magnetite nanoparticles as dual-targeting carriers for anticancer drug delivery. *Colloids Surf B: Biointerfaces* 2014;**117**:406-13.
3. Li J, He Y, Sun W, Luo Y, Cai H, Pan Y, et al. Hyaluronic acid-modified hydrothermally synthesized iron oxide nanoparticles for targeted tumor MR imaging. *Biomaterials* 2014;**35**:3666-77.
4. Chen H, Qi B, Moore T, Colvin DC, Crawford T, Gore JC, et al. Synthesis of brightly PEGylated luminescent magnetic upconversion nanophosphors for deep tissue and dual MRI imaging. *Small* 2014;**10**:160-8.
5. Yoo D, Jeong H, Noh SH, Lee JH, Cheon J. Magnetically triggered dual functional nanoparticles for resistance-free apoptotic hyperthermia. *Angew Chem Int Ed* 2013;**52**:13047-51.
6. Samanta B, Yan H, Fischer NO, Shi J, Jerry DJ, Rotello VM. Protein-passivated Fe_3O_4 nanoparticles: low toxicity and rapid heating for thermal therapy. *J Mater Chem* 2008;**18**:1204-8.
7. Ma Y, Liang X, Tong S, Bao G, Ren Q, Dai Z. Gold Nanoshell Nanomicelles for potential magnetic resonance imaging, light-triggered drug release, and photothermal therapy. *Adv Funct Mater* 2013;**23**:815-22.
8. Yang J, Shen D, Zhou L, Li W, Li X, Yao C, et al. Spatially confined fabrication of Core–Shell gold nanocages@ mesoporous silica for near-infrared controlled photothermal drug release. *Chem Mater* 2013;**25**:3030-7.
9. Shen S, Tang H, Zhang X, Ren J, Pang Z, Wang D, et al. Targeting mesoporous silica-encapsulated gold nanorods for chemo-photothermal therapy with near-infrared radiation. *Biomaterials* 2013;**34**:3150-8.
10. Wang Y, Black KC, Luehmann H, Li W, Zhang Y, Cai X, et al. Comparison study of gold nanohexapods, nanorods, and nanocages for photothermal cancer treatment. *ACS Nano* 2013;**7**:2068-77.
11. Yang K, Zhang S, Zhang G, Sun X, Lee S-T, Liu Z. Graphene in mice: ultrahigh in vivo tumor uptake and efficient photothermal therapy. *Nano Lett* 2010;**10**:3318-23.
12. Robinson JT, Tabakman SM, Liang Y, Wang H, Sanchez Casalongue H, Vinh D, et al. Ultrasmall reduced graphene oxide with high near-infrared absorbance for photothermal therapy. *J Am Chem Soc* 2011;**133**:6825-31.
13. Singh R, Torti SV. Carbon nanotubes in hyperthermia therapy. *Adv Drug Deliv Rev* 2013;**65**:2045-60.
14. Wang L, Shi J, Jia X, Liu R, Wang H, Wang Z, et al. NIR−/pH-responsive drug delivery of functionalized single-walled carbon nanotubes for potential application in cancer chemo-photothermal therapy. *Pharm Res* 2013;**30**:2757-71.
15. Wang QH, Kalantar-Zadeh K, Kis A, Coleman JN, Strano MS. Electronics and optoelectronics of two-dimensional transition metal dichalcogenides. *Nat Nanotechnol* 2012;**7**:699-712.
16. Liu T, Wang C, Gu X, Gong H, Cheng L, Shi X, et al. Drug delivery with PEGylated MoS_2 Nano-sheets for combined photothermal and chemotherapy of cancer. *Adv Mater* 2014;**26**:3433-40.
17. Cheng L, Liu J, Gu X, Gong H, Shi X, Liu T, et al. PEGylated WS_2 nanosheets as a multifunctional theranostic agent for in vivo dual-modal CT/photoacoustic imaging guided photothermal therapy. *Adv Mater* 1886-1893;**2014**:26.
18. Fan Q, Cheng K, Hu X, Ma X, Zhang R, Yang M, et al. Transferring biomarker into molecular probe: melanin nanoparticle as a naturally active platform for multimodality imaging. *J Am Chem Soc* 2014;**136**:15185-94.
19. Sun Y, Hong S, Ma X, Cheng K, Wang J, Zhang Z, et al. Recyclable Cu (I)/melanin dots for cycloaddition, bioconjugation and cell labelling. *Chem Sci* 2016;**7**:5888-92.
20. Zhang R, Fan Q, Yang M, Cheng K, Lu X, Zhang L, et al. Engineering melanin nanoparticles as an efficient drug-delivery system for imaging-guided chemotherapy. *Adv Mater* 2015;**27**:5063-9.
21. Fan Q, Cheng K, Yang Z, Zhang R, Yang M, Hu X, et al. Perylene-Diimide-based nanoparticles as highly efficient photoacoustic agents for deep brain tumor imaging in living mice. *Adv Mater* 2015;**27**:843-7.
22. Chu M, Shao Y, Peng J, Dai X, Li H, Wu Q, et al. Near-infrared laser light mediated cancer therapy by photothermal effect of Fe_3O_4 magnetic nanoparticles. *Biomaterials* 2013;**34**:4078-88.
23. Chen H, Burnett J, Zhang F, Zhang J, Paholak H, Sun D. Highly crystallized iron oxide nanoparticles as effective and biodegradable mediators for photothermal cancer therapy. *J Mater Chem B* 2014;**2**:757-65.
24. Shen S, Kong F, Guo X, Wu L, Shen H, Xie M, et al. CMCTS stabilized Fe_3O_4 particles with extremely low toxicity as highly efficient near-infrared photothermal agents for in vivo tumor ablation. *Nanoscale* 2013;**5**:8056-66.

25. Shirakura T, Kelson TJ, Ray A, Malyarenko AE, Kopelman R. Hydrogel nanoparticles with thermally controlled drug release. *ACS Macro Lett* 2014;**3**:602-6.
26. Cai L, Wen Y, Lin Z. Synthesis and characterization of dual-magnetic thermosensitive microspheres. *Adv Mater Res* 2011:1867-72.
27. Wang H, Luo W, Chen J. Fabrication and characterization of thermoresponsive Fe_3O_4@PNIPAM hybrid nanomaterials by surface-initiated RAFT polymerization. *J Mater Sci* 2012;**47**:5918-25.
28. Pan Y, Zhang Le, Zeng L, Ren W, Xiao X, Zhang J, et al. Gd-based upconversion nanocarriers with yolk-shell structure for dual-modal imaging and enhanced chemotherapy to overcome multidrug resistance in breast cancer. *Nanoscale* 2016;**8**:878-88.
29. Lee J, Park JC, Song H. A nanoreactor framework of a Au@SiO_2 yolk/shell structure for catalytic reduction of p-nitrophenol. *Adv Mater* 2008;**20**:1523-8.
30. Wang DP, Zeng HC. Multifunctional roles of TiO_2 nanoparticles for architecture of complex Core-shells and hollow spheres of SiO_2-TiO_2-Polyaniline system. *Chem Mater* 2009;**21**:4811-23.
31. Wu X-J, Xu D. Formation of yolk/SiO_2 Shell structures using surfactant mixtures as template. *J Am Chem Soc* 2009;**131**:2774-5.
32. Cheng L, Yang K, Li Y, Zeng X, Shao M, Lee S-T, et al. Multifunctional nanoparticles for upconversion luminescence/MR multimodal imaging and magnetically targeted photothermal therapy. *Biomaterials* 2012;**33**:2215-22.
33. Shen S, Guo X, Wu L, Wang M, Wang X, Kong F, et al. Dual-core@shell-structured Fe_3O_4-$NaYF_4$@TiO_2 nanocomposites as a magnetic targeting drug carrier for bioimaging and combined chemo-sonodynamic therapy. *J Mater Chem B* 2014;**2**:5775-84.
34. Guo X, Wu Z, Li W, Wang Z, Li Q, Kong F, et al. Appropriate size of magnetic nanoparticles for various Bioapplications in cancer diagnostics and therapy. *ACS Appl Mater Interfaces* 2016;**8**:3092-106.